# The Intra-Americas Sea springtime surface temperature anomaly dipole as fingerprint of remote influences

Ernesto Muñoz

*Cooperative Institute for Marine and Atmospheric Studies*
*Rosenstiel School for Marine and Atmospheric Science*
*University of Miami*
*Miami, FL, USA*

Chunzai Wang

*Atlantic Oceanographic and Meteorological Laboratory*
*National Oceanic and Atmospheric Administration*
*Miami, FL, USA*

David Enfield

*Cooperative Institute for Marine and Atmospheric Studies*
*Rosenstiel School for Marine and Atmospheric Science*
*University of Miami*
*Miami, FL, USA*

Corresponding author address: Ernesto Muñoz, CIMAS/RSMAS, University of Miami, 4600 Rickenbacker Causeway, Miami, FL 33149

E-mail: Ernesto.Munoz@noaa.gov

## Abstract

The influence of teleconnections on the Intra-Americas Sea (IAS; Gulf of Mexico and Caribbean Sea) has been mostly analyzed from the perspective of the El Niño-Southern Oscillation (ENSO) on the Caribbean Sea (the latter being an extension of the tropical North Atlantic). This emphasis has overlooked: 1) the influence of other teleconnections on the IAS and 2) which teleconnections affect the Gulf of Mexico climate variability. In this study we analyze the different fingerprints that major teleconnection patterns have on the IAS during boreal spring. Indices of teleconnection patterns are regressed and correlated to observations of oceanic temperature and atmospheric data from reanalyses and observational data sets. We find that the Pacific teleconnection patterns that influence the IAS SSTs do so affecting the Gulf of Mexico in an opposite manner to the Caribbean Sea. These Pacific climate patterns analyzed are the Pacific North American (PNA) teleconnection, the Pacific Decadal Oscillation (PDO) and ENSO. The North Atlantic Oscillation (NAO) is related to a lesser degree with the north-south SST anomaly dipole than are Pacific teleconnection patterns. We also find that the IAS influence from the midlatitude Pacific affects mostly the Gulf of Mexico whereas the influence from the tropical Pacific affects mostly the Caribbean Sea. Therefore, the combination of a warm ENSO event and a positive PNA event induces a strong IAS SST anomaly dipole between the Gulf of Mexico and the Caribbean Sea during spring.

By calculating an index that represents the IAS SST anomaly dipole we find that the dipole forms mostly in response to changes in the air-sea heat fluxes. In the Gulf of Mexico the dominant mechanisms are the air-sea differences in humidity and temperature. The changes in shortwave radiation also contribute to the dipole of net air-sea heat flux. The changes in shortwave radiation arise, in part, by the cloudiness triggered by the air-sea differences in

humidity, and also by the changes in the convection cell that connects the Amazon basin to the IAS. Weaker Amazon convection (e.g., in the event of a warm ENSO event) reduces the subsidence over the IAS and henceforth the IAS cloudiness increases (and the shortwave radiation decreases). This study contributes to a greater understanding of how the IAS is influenced by different Pacific and Atlantic teleconnections.

## 1. Introduction

In addition to Atlantic influence, the springtime tropical North Atlantic (TNA) sea surface temperature anomalies (SSTAs) are remotely forced by tropical Pacific SSTAs, in particular anomalies related to El Niño-Southern Oscillation (ENSO) (Enfield and Mayer, 1997; Saravanan and Chang, 2000). Enfield and Mayer (1997) observed that in response to wintertime Pacific warm ENSO events, the TNA SSTAs warm up during boreal spring as a result of the weakening of the North Atlantic Subtropical High (NASH) and the associated easterlies. The weakening of the TNA low-level easterlies, including those in the Caribbean Sea, results in decreased latent heat loss that warms the ocean mixed layer (Alexander and Scott, 2002) and decreased mixing of mixed layer water with cooler subsurface water (Enfield and Mayer, 1997). Additionally, during the month of January, the air-sea difference in humidity contributes to the latent heat flux anomalies in the Caribbean Sea (Chikamoto and Tanimoto, 2005). In the Gulf of Mexico, changes in the subtropical jet and the storm tracks associated with ENSO may affect the moisture availability (Coleman and Rogers, 2007). It is known that with El Niño (La Niña), the storm tracks and frontal passages are displaced farther south (north) along the Gulf coast (Compo and Sardeshmukh, 2004; Eichler and Higgins, 2005).

Together, the Caribbean Sea (CBN) and the Gulf of Mexico (GMX) are called the Intra-Americas Sea (IAS). However, the focus of many previous studies has been on the relation of ENSO to TNA SSTAs. The factors related to the Gulf of Mexico SSTAs have been comparatively understudied. Because springtime forcing of the ocean mixed layer is critical to the development of summer warm pool anomalies, an improved understanding of the processes during spring is desirable. Furthermore, questions remain as to what other teleconnections (aside

from ENSO) influence the IAS climate variability during early spring. Several studies have analyzed the IAS variability in summer and its impact (e.g., Muñoz et al. 2008; Wang et al. 2008). However, IAS forcing during boreal spring is a critical factor in determining the size and intensity of the summer Atlantic warm pool (Enfield et al. 2006, Lee et al. 2008), which in turn influences rainfall and tropical cyclones during the ensuing summer (Wang et al. 2008).

Also relevant to the IAS is the Pacific North American (PNA) pattern, which has an extension over the Florida peninsula that may influence the IAS climate anomalies. At longer timescales, the Pacific Decadal Oscillation (PDO) is another Pacific mode of variability that could influence the IAS as it has been observed to influence temperature and precipitation over northern South America (Dettinger et al, 2001; Mantua and Hare, 2002). A complicating factor is that the Pacific climate modes are not fully orthogonal to each other; ENSO is correlated in time with the PNA and spatially with the PDO. Hence, attempts to separate their respective impacts on IAS SSTAs must proceed with caution.

Changes in the Amazon convection may also influence the IAS during boreal spring. During springtime the Amazon convection is part of the atmospheric meridional overturning circulation that has a sinking branch over the tropical and subtropical North Atlantic and its changes may in turn be reflected in the TNA atmosphere. The changes in convection over the Amazon have been explained as a response to subsidence and stabilization of the upper troposphere (Lintner and Chiang, 2007) as well as to changes in diabatic heating due to other factors (e.g., Koren et al. 2004). The Amazon convection is subject to the influence of ENSO anomalies and may be another conduit by which ENSO events affect the TNA atmosphere (Mestas-Nuñez and Enfield, 2001; Wang, 2002, 2004; Chiang and Sobel, 2002).

The North Atlantic Oscillation (NAO) is another major teleconnection mechanism of the

northern hemisphere winter and whose influence may extend into the spring season. However, its nature has been ascribed to either atmospheric internal variability or forced by Atlantic SSTs (Czaja and Frankignoul, 2002; Okumura et al. 2001). Paeth et al (2003) finds that at intraseasonal timescales the NAO drives the North Atlantic SSTs but at longer timescales the North Atlantic SSTs drive the NAO.

The North Atlantic SSTAs show rich structures during boreal winter and spring. Deser and Timlin (1997) observed the dominant wintertime SSTA pattern at the intraseasonal timescale to be a SSTA tripole with positive nodes in the TNA (south of about 20°N) and in the high latitude North Atlantic (between 45°N and 65°N) opposing a middle antinode off the east coast of the United States. Tanimoto and Xie (2002) observed a similar pattern at the decadal timescale. In one phase, this North Atlantic tripole is reflected in the IAS as a dipole with positive SSTAs in the Caribbean Sea and negative SSTAs in the Gulf of Mexico (merging into the east coast antinode). Additionally, the IAS dipole has been observed in the spring following strong ENSO events (Alexander and Scott, 2002; Wang et al. 2004; Chikamoto and Tanimoto, 2005) and in the spring prior to anomalously large or small summer Western Hemisphere warm pools (Enfield et al. 2006). Some studies report a north-south dipole pattern of cloudiness and shortwave radiation anomalies over the IAS associated with ENSO (Curtis and Hastenrath, 1995; Klein et al. 1999; Lau and Nath, 2001). The IAS SSTA dipole, however, has been an overlooked feature of the IAS variability and merits further study.

In this study we analyze the IAS SSTA dipole between the Caribbean Sea and the Gulf of Mexico during late winter and early spring. Furthermore, we focus on the teleconnections to the IAS based on the SSTA dipole.

## 2. Data

To capture the IAS SSTA dipole, ERSST.v3 SST data (Smith et al. 2008) was used for the period 1949-2006. Based on the comprehensive ocean-atmosphere data set (COADS) from 1945-1993 (Woodruf et al. 1987) and the international COADS from 1960-2002, Wang et al. (2006) derived a data set that was interpolated to a regular grid of 1° latitude × 1° longitude. From this derived data set, the 1949-2002 turbulent and radiative heat fluxes between the air and the sea and surface wind stress and its curl were used. Other atmospheric fields analyzed here include precipitation from the University of Delaware (Willmott and Matsuura, 2007) and 250-hPa velocity potential and 500-hPa vertical pressure velocity from NCEP/NCAR reanalysis (Kalnay et al, 1996). The Simple Ocean Data Assimilation (SODA; Carton and Giese, 2008) is an ocean reanalysis data set with velocity, salinity and temperature at various depths. The version of the SODA used for this study was version 2.0.2 and was analyzed in the context of the subsurface anomalies related to the IAS dipole. For all the variables mentioned above, monthly anomalies were obtained by subtracting the 1971-2000 climatologies.

The COADS-derived heat fluxes are displayed following the convention that the net heat flux (Qnet, positive downward) is computed as: Qnet = SW – LW – LH – SH, where SW is shortwave radiation, LW is longwave radiation, LH is latent heat flux, SH is sensible heat flux and fluxes are positive into the ocean. The bulk formulas for turbulent heat fluxes are dependent on the wind speed (W) and the air-sea difference of humidity, δq (for LH), and of temperature, δT (for SH). These formulas can be decomposed into their time-mean and deviation from the mean ( ' ) to obtain SH = c(W'δT + Wδ$T'$) and LH = c(W'δq + Wδ$q'$), where c is a non-dimensional constant. The flux decomposition neglects the nonlinear terms (W’δT’ or W’δq’)

that are smaller. The decompositions of the turbulent heat fluxes were regressed onto the dipole index.

Teleconnection indices were obtained from NOAA CPC and ESRL websites. The following indices were used for these analyses: Pacific North American (PNA) pattern, Niño3.4 SSTA index, Equatorial Southern Oscillation index (EQSOI), Pacific Decadal Oscillation (PDO) and North Atlantic Oscillation (NAO) index. The Pacific Meridional Mode (PMM) index (Chiang and Vimont, 2004) was also used. The Atlantic Multidecadal Oscillation (AMO) index was derived by averaging the detrended SSTAs in the North Atlantic region (Enfield et al. 2001). The anomalies were calculated based on the 1951-1980 climatology, detrended by calendar month (based on the 1860 to 2002 trend) and smoothed with an 11-year low-pass filter. Finally, the smoothed and detrended SSTAs were averaged from 5°N to 65°N and from the eastern boundary (excluding the Mediterranean Sea) to the western boundary of the Atlantic (including the Gulf of Mexico) to obtain the AMO index. A similar SSTA-area index but for the 11-year high-pass anomalies was also calculated.

Considering the relation between the PNA and ENSO we calculate the correlation between the PNA and Niño3.4 indices used here. Even though the PNA has been described as the midlatitude manifestation of the ENSO signal (Wallace and Gutzler, 1981), there is only a moderate correlation between these two indices. The concurrent correlation between the Niño3.4 and PNA indices is highest during March with a significant correlation of 0.48. The lagged correlation is highest whenever the March PNA index is used (e.g., Niño3.4 in January and PNA in March) but is still below 0.45. The correlation throughout the rest of the winter and spring months (December, January, February and April) is between 0.30 and 0.24. This low correlation is not surprising given that some studies have identified the PNA and ENSO as separate modes

of variability during winter (Rodionov and Assel, 2001; Nigam, 2003) and early spring. That is to say, the PNA is an internal mode of atmospheric variability whose rate of occurrence is modestly or not affected by remote forcing from ENSO (Trenberth et al. 1998; Straus and Shukla, 2002). The PDO, however, correlates more highly with the PNA. From January through April the correlation of the PDO and the PNA (0.58) is greater than that between the PDO and Niño3.4 (0.44). However, the significant levels between these correlations are different because the decorrelation timescale of the Niño3.4 index is shorter than the decorrelation timescale of the PDO index. After calculating the effective correlation (by taking into account the autocorrelation of each of the indices (see Sciremammano, 1979)), the correlation between the PDO and the Niño3.4 is 3.8 times their effective correlation, and that between the PDO and the PNA is 3.55 times their effective correlation, indicating a slightly stronger correlation between the PDO and the Niño3.4 indices.

**3. The IAS dipole**

The correlation between SSTAs in the Gulf of Mexico and in the Caribbean Sea for the different seasons shows a cycle with negative correlation that peaks in late winter and early spring and positive correlations that peak in late summer and early fall (Table 1). The Caribbean SSTA index (CBN) was constructed by averaging the SSTAs in the domain (66-88°W, 12-20°N). For the Gulf of Mexico (GMX) the SSTAs were averaged within (76-96°W, 22-32°N). The Pacific was not included when calculating the area averages. To determine whether a SSTA dipole in the IAS is statistically significant we quantify the chi-square statistic from a contingency table. Data for month of March were used. A contingency table and the derived statistic are used to analyze the degree of independence of two variables.

Contingency tables have been used, for example, in the context of the tropical Atlantic dipole (interhemispheric mode) by Enfield et al (1999). For the present study, the two variables were the Caribbean SSTAs and the Gulf of Mexico SSTAs.

The contingency table was constructed using terciles of the CBN and GMX indices for the 58 years from 1949 to 2006. Table 2 shows the number of cases in each category. The contingency table statistics were computed with the VassarStats Website for Statistical Computation. For the present combinations there are four degrees of freedom and the chi-square statistic at the 5% level of significance should be greater than 9.49 to reject the null hypothesis that the CBN SSTAs are independent of the GMX SSTAs. The expected frequency was greater than five for more than 80% of the table cells, which renders the chi-square statistic valid. For the contingency table, the chi-square was 19.53 and the null hypothesis is rejected. This indicates that the table shows contingency between the two variables and that the CBN and GMX SSTAs are not independent, their relation being one of opposition to each other.

Next we calculate an IAS SSTA dipole index and analyze it with respect to the climate anomalies related to it. The IAS SSTA dipole index was calculated as the difference of March SST standardized anomalies in the Caribbean minus the Gulf of Mexico (CBN-GMX) for those years in which the SSTAs in either basin are of opposite sign to those of the other basin. To identify the dipole years we construct a mask that takes into consideration the difference and sum of the CBN and GMX indices with the following formula: abs( (CBN-GMX) / (CBN+GMX) ) - 1.0 . The years for which the mask is less than zero are not taken into account in the dipole index and are categorized as non-dipole years. The CBN and GMX SSTA indices for the dipole years and the non-dipole years are presented in Figure 1. The IAS dipole index results in a time series with small to large IAS dipoles that are in some years symmetrical and other years

dominated by either basin.

Figure 2 shows the correlation between the IAS SSTA dipole index and SSTAs from February to April. The non-dipole years were not included and therefore the degrees of freedom were estimated by the number of dipole years minus one. The dipole is evident with cold SSTAs in the Gulf of Mexico and opposing SSTAs in the Caribbean Sea. The Caribbean Sea SSTAs are part of a larger anomalous SSTA pattern that crosses the TNA from the east to the west. (In the tropical South Atlantic (TSA), however, there are no SSTAs suggesting that the IAS dipole may not be related to TSA variability.) The Gulf of Mexico SSTAs are also related to anomalies that extend to the east until about 40°W and to the north. Corroboration of the SSTA dipole was done with other data sets such as HadISST (Rayner et al, 2003) and SODA (Carton and Giese, 2008). The statistically significant SSTAs in the Pacific and Indian Oceans are an indication that the dipole is related to teleconnections.

The atmospheric low-level circulation anomalies associated with the dipole are shown in Figure 3. There are cyclonic anomalies in the mid-latitude North Atlantic and also in the higher latitudes of the North Pacific (the Aleutian low region). These are separated by moderate pressure anomalies over the North American continent. Consequently, the 850-hPa wind over the IAS weakens with respect to the normal flow over the GMX (southerly) and CBN (easterly). In the tropical Pacific the westerly wind anomalies corresponding to a warm ENSO event can also be appreciated. In the midlatitude Pacific the North Pacific node of the PNA pattern stands out.

Figure 4 shows the correlation coefficients between several teleconnection indices and the IAS dipole index. In March, the dipole is highly correlated with several teleconnection indices including the Niño3.4 (r=0.71), the PNA (r=0.58) and the PDO (r=0.66). However,

although statistically significant the correlation with the NAO (r=-0.37) is not as high as that with the Pacific indices. The AMO index calculated for this study has a low correlation (r<0.10) with the dipole index. But the 11-year high-pass North Atlantic SSTA index is highly correlated with the dipole index.

Shown in Figure 5 are the SST anomalies associated with the two North Atlantic SSTA indices (the low-pass (AMO) and the high-pass indices). The low-pass index confirms the association with the AMO showing a multi-decadal behavior and same-sign anomalies over the North Atlantic in general. The high-pass index shows an SSTA tripole in the North Atlantic (and its corresponding SSTA dipole in the IAS) and large SST anomalies in the tropical Pacific. The North Atlantic high-pass index has a correlation of 0.58 with the Niño3.4 index when the Niño3.4 index leads by two months. This indicates that the high-correlation between the North Atlantic high-pass index and the dipole index shows the inter-correlation with the Niño3.4. The remote forcings will be discussed in more detail in the following sections. As there are teleconnections that lead the dipole index we focus on the anomalies of atmospheric circulation and air-sea fluxes that lead the IAS SST anomalies.

**4. Formation of the IAS SSTA dipole**

The associated net heat flux anomalies leading the dipole (Figure 6e) also have a dipole structure with positive (downward) anomalies over the Caribbean and TNA and negative (upward) anomalies over the Gulf of Mexico and eastern coast of the USA. In the Gulf of Mexico, from the turbulent and radiative heat fluxes the main contributor is the latent heat flux (Figure 6a). When the latent heat flux is decomposed (see section 2) and its components are regressed onto the dipole index (Table 3), it becomes evident that the component that contributes

the most in the Gulf of Mexico is Wδq'. The sensible heat flux also has a large contribution to the SSTA dipole in the Gulf of Mexico region (Figure 6b) and the term that dominates in the Gulf of Mexico is the δT' term. In the Caribbean, the regression values of sensible heat flux are small and neither term dominates. Although also with small latent heat flux anomalies in the Caribbean, the Wδq' term contributes the most to the positive latent heat flux anomalies. The Wδq' contribution in the Caribbean was also found by Chikamoto and Tanimoto (2005) to be significant.

In the Gulf of Mexico the surface winds blow mainly in the meridional direction (Figure 6f) which coupled to the stronger meridional gradient of humidity renders the Wδq' component of the latent heat flux as the dominant. As the northerly wind anomalies north of and in the Gulf of Mexico inhibit the transport of moisture to the continental USA and advect dry air from the north, the air-sea difference in moisture triggers heat fluxes that ultimately cool the SSTs in the Gulf of Mexico. In the IAS during springtime there is also a meridional gradient of SST and surface air temperature. Hence, following the rationale of Cayan (1992), the δq' and δT' terms have more prominence in the Gulf of Mexico as it is in this region where the wind anomalies are stronger in the meridional direction (Figure 3).

The correlation between the dipole index and IAS subsurface temperature is significant when the subsurface temperature anomalies lag the dipole index. However, the correlation is not significant when the subsurface temperature anomalies lead the dipole index. The lag of subsurface temperature anomalies indicates that air-sea interactions are the principal conduit by which the IAS is forced during late winter and early spring.

For the case of a higher air-sea moisture difference in the Gulf of Mexico during the IAS SSTA dipoles, the cloudiness increases. This aspect is reflected in the shortwave radiation

anomalies (Figure 6c). Negative shortwave anomalies are more prominent over the Gulf of Mexico and western Caribbean and centered near the Yucatan channel and the Straits of Florida. The increase in cloudiness would in turn cool the surface waters of the Gulf of Mexico as it blocks the shortwave radiation penetration. But in the western Caribbean Sea this is offset by the increase in longwave radiation. In the eastern Caribbean Sea, the shortwave radiation still penetrates and the latent heat flux also acts to warm the sea. Associated with the surface wind anomalies are downwelling anomalies along the South American coast in the eastern part of the Caribbean (Figure 6f), which also contribute to the warming of the SSTs.

The negative shortwave anomalies are collocated with an increase in upper-level divergence indicating an anomalous rising branch in the atmospheric circulation over the IAS (Figure 7 top). The corresponding anomalous sinking branch lies over the eastern Amazon basin and western deep tropical Atlantic (i.e., 35-65°W, 5°S-15°N).

## 5. Teleconnections

*(a) Divergent circulation*

Boreal winter and spring are the seasons when the convection over the Amazon is stronger and closer to the equator during spring. In the climatology, the convection cell has a sinking branch stronger over the TNA and a weaker sinking branch over the IAS. However, when the IAS SSTA dipole index is regressed on atmospheric circulation fields, the relationship between the Amazon region and the IAS stands out (Figure 7). Even though there are also divergent wind anomalies connecting the easternmost equatorial Pacific with the Amazon basin, the February-March anomalies of the divergent wind are stronger between the IAS and the Amazon basin (Figure 7, top). These relationships confirm that the precipitation and convection

anomalies over the Amazon region are related to the IAS, in this case the IAS dipole during spring.

Before the mature phase of the IAS dipole in March, the December-January vertical velocity anomalies show an upward anomaly over the IAS (stronger over the northeast of the Greater Antilles). The divergent wind anomalies aloft diverge from that region and converge over northeastern South America (over the eastern Amazon basin) and the western TNA between the equator and 10°N. In those regions there are subsidence anomalies and a decrease in precipitation as expected from the changes in the Pacific. At the lower levels, the divergent circulation (not shown) is directed from northeastern South America towards the IAS, closing the circulation cell. The inhibition of convection over the Amazon is also a response to the weakening of the Atlantic trade winds that at this time of the year carry moisture to the Amazon region. By having less humidity in the region, less convection develops.

A separate circulation cell that connects the IAS to the Midwest of the USA develops in February-March. The upward velocity anomaly over the Caribbean has a descending counterpart over the Midwest and strong irrotational wind anomalies diverge from the IAS and converge over the Midwest. In fact, the precipitation over the Midwest region decreases whereas it increases over the Florida peninsula. As we have discussed above, this circulation cell also extends to the lower levels where the irrotational circulation anomalies are in the opposite sense as those aloft. (It is important to remember that the results discussed above come from the regression of the dipole index onto climatic fields and that the dipole index is correlated not only to ENSO but also to other teleconnection patterns.) In fact, the convection anomaly over the IAS may also be related to the low-pressure anomaly of the PNA wavetrain that reaches the IAS.

*(b) ENSO vs. PNA*

To distinguish between the influence of the PNA and that of the equatorial Pacific anomalies on the IAS SST anomalies, an analysis was done from a sample of the Niño3.4 index that excludes 20 March extreme events of the PNA index. The March PNA extreme events excluded are the 10 most negative events: 1954, 1955, 1963, 1964, 1967, 1976, 1982, 1989, 1997, 2002; and the 10 most positive events: 1957, 1973, 1981, 1983, 1984, 1986, 1987, 1993, 1998, 2000. Then the values of the Niño3.4 and PDO indices corresponding to those PNA extreme events were removed from their time series to create no-extreme-PNA (no_pna) Niño3.4 and PDO indices. The no_pna Niño3.4 index was regressed and correlated to SSTAs in the Atlantic and Pacific basins as shown in Figure 8a. For no_pna years the Niño3.4 index has a positive relation with the Caribbean SSTAs from January, peaking in March and extending across the TNA in April. The Gulf of Mexico SSTAs are not as significantly related to the Niño3.4 except in February when the Gulf of Mexico shows cool anomalies as part of a greater area of negative SSTAs that extend to the western North Atlantic region.

The identification of the years when the March Niño3.4 values were extreme was also done. The 10 years when the March Niño3.4 values were the most negative were 1950, 1951, 1955, 1956, 1971, 1974, 1985, 1989, 1999, 2000 and the 10 years when the March Niño3.4 values were the most positive were 1958, 1966, 1969, 1973, 1983, 1987, 1992, 1993, 1998, 2003. These years were removed from the PNA index and the no-extreme-N34 (no_n34) PNA index was analyzed with respect to SSTAs. When there are no extreme Niño3.4 events in March, the PNA and PDO indices stay significantly correlated at 0.51. However, the correlation between the Niño3.4 index and the PNA (and the PDO) drops from 0.48 to 0.19 (from 0.47 to 0.16). Henceforth, the regression of the no_n34 PNA index onto the IAS climate variables has

removed some of the ENSO influence on the IAS that is mediated by the PNA. Figure 8b shows the no_n34 PNA index regressed onto SSTAs for the Pacific and Atlantic basins. It can be observed that the PNA influence is mostly on the Gulf of Mexico in March and April. Essentially, during March and April ENSO influences mostly the Caribbean region, and the PNA influences mostly the Gulf of Mexico region. Therefore, when a warm winter-spring ENSO event combines with a positive spring PNA event, the IAS shows a strong dipole of SSTAs with cooler SSTAs in the Gulf of Mexico and warmer SSTAs in the Caribbean Sea and TNA.

The PDO also has a relation to the IAS dipole (Figure 8c). However, the PDO's relation varies depending on the strength of the PNA and ENSO. To distinguish between the influence of the PNA and the influence of the Niño3.4 with respect to the PDO, a comparison was done after calculating the partial correlation of the PDO index and SST anomalies by controlling the PNA index or the Niño3.4 index. Figure 8c shows the difference in March-April explained variance of the PDO when the PNA is controlled minus when the Niño3.4 is controlled. It is clear that in the Gulf of Mexico the PDO index has *greater* explained variance when the Niño3.4 index is controlled versus when the PNA index is controlled. However, in the Caribbean and the TNA the PDO index has *less* explained variance when the Niño3.4 index is controlled versus when the PNA index is controlled. This, again, indicates a greater association between PNA and the Gulf of Mexico variability, and between Niño3.4 and the Caribbean Sea variability.

*(c) Time-scale distinctions*

To further explore the remote areas related to the IAS SSTA dipole we apply a 5-year temporal filter to the SSTAs and then recalculate the CBN-GMX difference of SSTAs obtaining a high-pass and a low-pass dipole indices. The 5-year high-pass dipole variability is strongly

related to ENSO tropical Pacific SSTAs (Figure 9 left column). The tropical Pacific SSTAs correspond to an ENSO event that decays by late spring but that still has significant SSTAs during early spring. The anomalies in the Gulf of Mexico are stronger in March and are significant throughout the spring season until May. However, the Caribbean SSTAs extend longer from January to July. This is probably related to the difference on how the Gulf of Mexico and the Caribbean Sea are forced. The Gulf of Mexico is essentially forced by the meridional advection of dryer air associated to the winter frontal passages occurring across the southern tier of US states. This variation in storm tracks is mostly in association to Pacific variability during the winter to early spring months. The Caribbean and the TNA respond mostly to the easterly low-level wind anomalies, which have more to do with the NASH and which are thus not limited to the early months of the year but can occur throughout the year. That is to say, the longer persistence of Caribbean SSTAs is likely due to positive ocean-atmosphere feedback within the tropical Atlantic.

The 5-year low-pass IAS dipoles are not as strong in the IAS as they are between the oceanic region east of the US and the Caribbean-TNA. Also, they are not related to ENSO anomalies (Figure 9 right column). They are mostly related to a band of Pacific SSTAs that extends from the subtropical central Pacific to the western coast of the USA. Associated with the development of this band there is also a region of opposing SSTAs to its northwest centered at about 160°W and 35°N. This pattern is similar to the one identified by Chiang and Vimont (2004) as the Pacific Meridional Mode. In fact, the correlation of the low-pass IAS dipole index and the PMM is 0.55. Also, Paegle and Mo (2002) identified a similar pattern in December-February (Figure 12d of Paegle and Mo, 2002) associated with latitudinal variations of precipitation over South America.

The subsurface temperature anomalies associated with the high-pass and low-pass IAS dipole indices are shown in Figure 10. Related to the high-pass dipole the temperature anomalies are consistently warm in the Caribbean basin from the surface to about 300 meters. Similarly north of the Caribbean basin the temperature anomalies are consistently cool down to about 200 meters. These anomalies extend to the summer season. However, related to the low-pass IAS dipole index the subsurface temperature anomalies are not consistent with depth. The surface warming of the Caribbean extends down to about 100 meters. But farther down there are cool anomalies opposing the surface warming. However, the cooling north of the Caribbean is consistent with depth and extends to 300 meters.

## 6. Summary and conclusions

Statistical analysis of the variability of SSTAs in the Intra-Americas Sea region during springtime has shown that the IAS has as a main mode of variability an SSTA dipole between the Gulf of Mexico and the Caribbean Sea. Associated with the IAS SSTA dipole are northerly surface wind anomalies that blow from the colder Gulf of Mexico to the warmer Caribbean Sea, and westerly wind anomalies over the Caribbean. This dipole is mainly forced by air-sea turbulent and radiative fluxes with the latent heat flux and the shortwave radiation having the greater influence with a lead of two months. The IAS SSTA dipole is the manifestation of various teleconnections, responding most strongly to the combination of a positive PNA event and a warm ENSO event.

In general, IAS dipole events are established by influences from the mid-latitude Pacific and the tropical Pacific. The SSTAs in the Gulf of Mexico are mainly influenced by the PNA

and the PDO, whereas those of the Caribbean Sea and the TNA are mainly influenced by ENSO. A warm winter-spring ENSO event reflects as warm SSTAs in the Caribbean Sea and the TNA (Enfield and Mayer, 1997; Saravanan and Chang, 2000). A positive PNA and positive PDO are both related to cool temperatures in the Gulf of Mexico. The influence of the PNA does not reach as far south in the IAS to affect the Caribbean Sea SSTs except when concurrent with warm ENSO conditions.

The contribution of the latent heat flux anomalies in the Gulf of Mexico is mainly due to the air-sea difference in humidity. The air-sea temperature difference is the aspect mostly responsible for the sensible heat flux contribution. The shortwave radiation contribution is a reflection of the changes in cloudiness associated with the dipole. With a cool Gulf of Mexico and a warm Caribbean Sea there is an increase of precipitation over the Gulf of Mexico and the central IAS. The increase of precipitation is related to the air-sea humidity difference as the cold air masses from the north encounter the Gulf of Mexico during positive PNA events and warm ENSO events. The positive anomalies of precipitation over the Gulf of Mexico are also related to a reduced local subsidence, owing to a decrease in convection over tropical South America and western tropical Atlantic. These relationships confirm that the changes in convection and precipitation over the Amazon are strongly linked to the changes in the IAS during late winter and early spring.

A tropical Pacific influence is felt through changes in the regional Hadley circulation that connects tropical South America with the TNA and the IAS. Essentially, as the tropical Pacific warms and the Amazon precipitation diminishes there is a weakening of the meridional overturning (Hadley) cell that connects tropical South America with the IAS-TNA and the NASH. The weakening of this Hadley cell manifests as an increase in precipitation over the IAS

(in particular the Gulf of Mexico). The increase in Gulf of Mexico precipitation also has contributions from the air-sea humidity difference (Cayan, 1992).

The modulation of the IAS SSTA dipole variability is also influenced by the PDO. The PDO has been described as a low-frequency signal apparently triggered by the white noise from atmospheric phenomena in the Pacific such as the PNA (Barsugli and Battisti, 1998). For the case of the IAS a similar response (i.e., a red oceanic signal as a result of the PNA white atmospheric forcing) may be occurring and henceforth the correlation of the IAS SSTA dipole with the PDO shows large values (greater than 0.6). Nonetheless, the response of the Gulf of Mexico to atmospheric white noise forcing from the PNA needs to be studied further.

In this study we have demonstrated that in addition to ENSO there are other Pacific teleconnections that influence the IAS climate variability during springtime. This is important with respect to prediction of climate anomalies in the IAS region.

***Acknowledgements***

This research was carried out [in part] under the auspices of the Cooperative Institute for Marine and Atmospheric Studies (CIMAS), a Cooperative Institute of the University of Miami and the National Oceanic and Atmospheric Administration, cooperative agreement #NA17RJ1226. This work was supported by the National Oceanic and Atmospheric Administration (NOAA) Climate Program Office and the base funding of NOAA Atlantic Oceanographic and Meteorological Laboratory (AOML). The findings and conclusions in this report are those of the author(s) and do not necessarily represent the views of the funding agency.

## References


Alexander, M.A. and J.D. Scott, 2002: The influence of ENSO on air-sea interaction in the Atlantic. *Geophys. Res. Lett.*, **29**, 1701, doi:10.1029/2001GL014347.

Alexander, M.A., C. Deser, and M.S. Timlin, 1999: The reemergence of SST anomalies in the North Pacific Ocean. *J. Climate*, **12**, 2419–2433.

Barsugli, J.J., and D.S. Battisti, 1998: The basic effects of atmosphere-ocean thermal coupling on midlatitude variability. *J. Atmos. Sci.*, **55**, 477-493.

Carton J.A. and B.S. Giese, 2008: A reanalysis of ocean climate using SODA, *Mon. Wea. Rev.*, **136**, 2999-3017.

Cayan, D.R., 1992: Latent and sensible heat flux anomalies over the northern oceans: The connection to monthly atmospheric circulation. *J. Climate*, **5**, 354-369.

Chang, P., L. Ji, and H. Li, 1997: A decadal climate variation in the tropical Atlantic Ocean from thermodynamic air–sea interactions. *Nature,* **385,** 516–518.

Chiang, J.C.H., and A.H. Sobel, 2002: Tropical tropospheric temperature variations caused by ENSO and their influence on the remote tropical climate. *J. Climate*, **15**, 2616–2631.

Chiang, J.C.H., and D.J. Vimont, 2004: Analogous meridional modes of atmosphere-ocean variability in the tropical Pacific and tropical Atlantic. *J. Climate*, **17**, 4143–4158.

Chikamoto, Y. and Y. Tanimoto, 2005: Role of specific humidity anomalies in Caribbean SST response to ENSO. *J. Meteor. Soc. Japan*, **83**, 959-975.

Coleman, J.S.M., and J.C. Rogers, 2007: A synoptic climatology of the central United States and associations with Pacific teleconnection pattern frequency. *J. Climate*, **20**, 3485-3497.

Compo, G.P., and P.D. Sardeshmuk, 2004: Storm track predictability on seasonal and decadal

scales. *J. Climate*, **17**, 3701-3720.

Curtis S., and S. Hastenrath, 1995: Forcing of anomalous sea surface temperature evolution in the tropical Atlantic during Pacific warm events. *J. Geophys. Res*, **100**, 15835-15847.

Czaja, A., and C. Frankignoul, 2002: Observed impact of Atlantic SST anomalies on the North Atlantic Oscillation. *J. Climate*, **15**, 606-623.

Deser, C. and M.S. Timlin, 1997: Atmosphere-ocean interaction on weekly timescales in the North Atlantic and Pacific. *J. Climate*, **10**, 393-408.

Dettinger, M.D., D.S. Battisti, G.J. McCabe, C.M. Bitz, and R.D. Garreaud, 2001: Interhemispheric effect of interannual and decadal ENSO-like climate variations on the Americas. *Interhemispheric climate linkages.* V. Markgraf, editor. Academic press. pp.1-12.

Eichler, T. and W. Higgins, 2006: Climatology and ENSO-related variability of North American extratropical cyclone activity. *J. Climate*, **19**, 2076-2093.

Enfield, D.B. and D.A. Mayer, 1997: Tropical Atlantic sea surface temperature variability and its relation to El Niño-Southern Oscillation. *J. Geophys. Res.*, **102**, 929-945.

Enfield, D.B, S.-K. Lee, and C. Wang, 2006: How are large Western Hemisphere Warm Pools formed? *Progr. Oceanogr.*, **70**, 346-365.

Enfield, D.B., A. M. Mestas-Nuñez and P.J. Trimble, 2001: The Atlantic multidecadal oscillation and its relation to rainfall and river flows in the continental U.S.. *Geophys. Res. Lett.*, **28**, 2077-2080.

Enfield, D.B., A.M. Mestas-Nuñez, D.A. Mayer and L. Cid-Serrano, 1999: How ubiquitous is the dipole relationship in tropical Atlantic sea surface temperatures? *J. Geophys. Res*., **104**, 7841-7848.

Kalnay, E., and co-authors, 1996: The NCEP/NCAR 40-Year Reanalysis Project. *Bull. Amer.*

*Meteor. Soc.*, **77**, 437–471.

Klein, S.A., B.J. Soden, and N.C. Lau, 1999: Remote sea surface temperature variations during ENSO: Evidence for a tropical atmospheric bridge. *J. Climate*, **12**, 917–932.

Koren, I., Y.J. Kaufman, L.A. Remer, and J.V. Martins, 2004: Measurement of the effect of Amazon smoke on inhibition of cloud formation. *Science*, **202**, 1342-1345.

Lee, S.-K., D.B. Enfield, and C. Wang, 2008: Why do some El Niños have no impact on tropical North Atlantic SST? *Geophys. Res. Lett.*, **35**, L16705, doi:10.1029/2008GL034734.

Lau, N.C., and M.J. Nath, 2001: Impact of ENSO on SST variability in the North Pacific and North Atlantic: Seasonal dependence and role of extratropical sea-air Coupling. *J. Climate*, **14**, 2846–2866.

Lintner, B.R., and J.C.H. Chiang, 2007: Adjustment of the remote tropical climate to El Niño conditions. *J. Climate*, **20**, 2544-2557.

Mantua, N.J., and S.R. Hare, 2002: The Pacific Decadal Oscillation. *J. Oceanogr.*, **58**, 35-44.

Mestas-Nuñez, A.M., and D.B. Enfield, 2001: Eastern equatorial Pacific SST variability: ENSO and non-ENSO components and their climatic associations. *J. Climate*, **14**, 391-402.

Muñoz, E., A.J. Busalacchi, S. Nigam and A. Ruiz-Barradas, 2008: Winter and summer structure of the Caribbean low-level jet. *J. Climate*, **21**, 1260-1276.

Nigam, S., 2003: Teleconnections. *Encyclopedia of Atmospheric Sciences*, J.R. Holton, J. Pyle and J. Curry, Eds., Academic Press, 2243–2269.

Okumura, Y., S.-P. Xie, A. Numaguti, and Y. Tanimoto, 2001: Tropical Atlantic air-sea interaction and its influence on the NAO. *Geophys. Res. Lett.*, **28**, 1507-1510.

Paegle, J.N., and K.C. Mo, 2002: Linkages between summer rainfall variability over South America and sea surface temperature anomalies. *J. Climate*, **15**, 1389-1407.

Paeth H., M. Latif and A. Hense, 2003: Global SST influence on twentieth century NAO variability. *Clim. Dyn.*, **21**, 63–75, doi:10.1007/s00382-003-0318-4

Rayner, N.A., P. Brohan, D.E. Parker, C.K. Folland, J.J. Kennedy, M. Vanicek, T. Ansell and S.F.B. Tett, 2006: Improved analyses of changes and uncertainties in sea surface temperature measured in situ since the mid-nineteenth century: the HadSST2 data set. *J. Climate*. **19**, 446-469.

Rodionov, S., and R. Assel, 2001: A new look at the Pacific/North American index. *Geophys. Res. Lett.*, **28**, 1519-1522.

Ruiz-Barradas, A., J.A. Carton and S. Nigam, 2000: Structure of interannual-to-decadal climate variability in the tropical Atlantic sector. *J. Climate*, **13**, 3285–3297.

Saravanan, R., and P. Chang, 2000: Interaction between tropical Atlantic variability and El Niño-Southern Oscillation. *J. Climate*, **13**, 2177-2194.

Sciremammano, F., 1979: A suggestion for the presentation of correlations and their significance levels. *J. Phys. Oceanogr.*, **9**, 1273-1276.

Smith, T.M., R.W. Reynolds, T.C. Peterson, and J. Lawrimore, 2008: Improvements to NOAA's Historical Merged Land-Ocean Surface Temperature Analysis (1880-2006). *J. Climate*, **21**, 2283-2296.

Straus, D.M., and J. Shukla, 2002: Does ENSO force the PNA? *J. Climate*, **15**, 2340–2358.

Tanimoto, Y., and S.-P. Xie, 2002: Inter-hemispheric decadal variations in SST, surface wind, heat flux and cloud cover over the Atlantic Ocean. *J. Meteor. Soc. Japan*, **80**, 1199-1219.

Trenberth, K.E., G.W. Branstator, D. Karoly, A. Kumar, N-C. Lau, and C. Ropelewski, 1998: Progress during TOGA in understanding and modeling global teleconnections associated with tropical sea surface temperatures. *J. Geophys. Res.*, **103**, 14291-14324.

Wallace, J.M., and D.S. Gutzler, 1981: Teleconnections in the geopotential height field during the Northern Hemisphere winter. *Mon. Wea. Rev.*, **109**, 784-812.

Wang, C., 2002: Atlantic climate variability and its associated atmospheric circulation cells. *J. Climate*, **15**, 1516-1536.

Wang, C., 2004: ENSO, Atlantic climate variability, and the Walker and Hadley circulations. In: Diaz, H.F., Bradley, R.S. (Eds.), *The Hadley Circulation: Present, Past, and Future*. Kluwer Academic Publishers, pp. 173-202.

Wang, C., S.-K. Lee, and D.B. Enfield, 2008: Climate response to anomalously large and small Atlantic warm pools during the summer. *J. Climate*, **21**, 2437–2450.

Wang, C., S.-P. Xie, and J. A. Carton, 2004: A global survey of ocean-atmosphere interaction and climate variability. *Earth's Climate: The Ocean-Atmosphere Interaction,* C. Wang, S.-P. Xie, and J.A. Carton, Eds., AGU Geophysical Monograph Series, No. 147, 1-19.

Wang, C., W. Wang, D. Wang, and Q. Wang, 2006: Interannual variability of the South China Sea associated with El Niño. *J. Geophys. Res.*, **111**, C03023, doi:10.1029/2005JC003333

Willmott, C. J. and K. Matsuura, 2007: Terrestrial Precipitation: 1900-2006 Gridded Monthly Time Series, http://climate.geog.udel.edu/~climate/html_pages/Global_ts_2007/README.global.p_ts_2007.html.

Woodruff, S.D., R.J. Slutz, R.L. Jenne and P.M. Steurer, 1987: A comprehensive ocean-atmosphere data set, *Bull. Amer. Meteor. Soc.*, **68**, 1239-1250.

**Figure Captions**

Figure 1. Time series of standardized SSTAs (°C) averaged over the Caribbean (blue) and the Gulf of Mexico (red) for IAS dipole years. The Caribbean area average is (66-88°W, 12-20°N) and the Gulf of Mexico area average is (76-96°W, 22-32°N) excluding the Pacific data.

Figure 2. February-to-April correlation between the IAS SSTA dipole index and SSTAs (°C) from 1949 through 2006. The contour interval is 0.2 starting at ±0.3. The long-dashed contour is the zero correlation contour.

Figure 3. February-March regression of IAS SSTA dipole index onto 850-hPa wind (m/s; vectors) and surface pressure (hPa; shades) from 1949 to 2006.

Figure 4. Correlation between the IAS SSTA dipole index and teleconnection indices in the Pacific (PDO, PNA, Nino3.4, EQSOI, PMM) and in the Atlantic (AMO, NAO, Natl 11-year high-pass).

Figure 5. (Top) Regression of SSTA (°C) onto 11-year low-pass (left) and high-pass (right) North Atlantic SSTA index from 1949 to 2001. Contour interval is 0.1°C. Positive values are in dark gray and solid contours. Negative values are in light gray and dashed contours. (Bottom) Time series of the 11-year low-pass (left) and high-pass (right) index. (See text for explanation of indices).

Figure 6. (a-e) January-to-March average regression (1949-2002) of turbulent and radiative air-sea heat fluxes ($W/m^2$) on dipole index (shades). Panels correspond to a) latent heat flux, b) sensible heat flux, c) shortwave, d) longwave, and e) net heat flux. The contours in panels a-e indicate the correlation at intervals of 0.2 starting at ±0.2 (negative correlations are shaded

and positive correlations are solid). The contours in panel e indicate the ±0.3°C SSTA regression values. Panel f shows the regression of wind stress (arrows; $10^{-2}$ N/m$^2$) and Ekman pumping (shades; meters/month). The reference arrow is $1x10^{-2}$ N/m$^2$.

Figure 7. (Top) Regression of IAS SSTA dipole index onto upper-level (250-hPa) divergent wind (vectors) and velocity potential anomalies (contours). The reference arrow is $10^{-1}$ m/s. Black vectors are significant at the 95% level. The shades correspond to where the correlations between the dipole index and the 500-hPa vertical pressure velocity anomalies are greater than 0.3 or less than -0.3. The contour interval for velocity potential is $3x10^5$ m$^2$/s. (Bottom) Regression of precipitation anomalies (mm/month) with the IAS dipole index. The white contours encompass the regions where the regression is statistically significant at the 95% level.

Figure 8. (a) March-April SSTA (°C) average regression of March Nino3.4 index when the March PNA extreme years have been excluded. (b) March-April SSTA (°C) average regression of March PNA index when the March Nino3.4 extreme years have been excluded. Contour interval is 0.2 starting at ±0.2. Values significant at the 95% level are shaded. (c) Difference in explained variance (%) of the March-April partial correlation between the PDO and SSTAs when the PNA index is controlled versus when the Nino3.4 index is controlled (see text for explanation). Contour interval is 2%. The zero contour has been omitted. Dark gray denotes positive values and light gray denotes negative values.

Figure 9. SSTA (°C) regression onto (left) 5-year high-pass dipole index and (right) 5-year low-pass dipole index for (from top to bottom) June-August of previous year, October-December of previous year, February-April and June-August. Contour interval is 0.2 starting at ±0.2. Values significant at the 95% level are shaded.

Figure 10. IAS zonal average of March (top) and July (bottom) regression of subsurface temperature (°C) for the 5-year high-pass (left) and low-pass (right) IAS spring dipole index. The zonal average is from the western boundary to 60°W. The black contours are the climatological isotherms (°C). The gray contours encompass the depths of significant regressions at the 95% level.

**Figures**

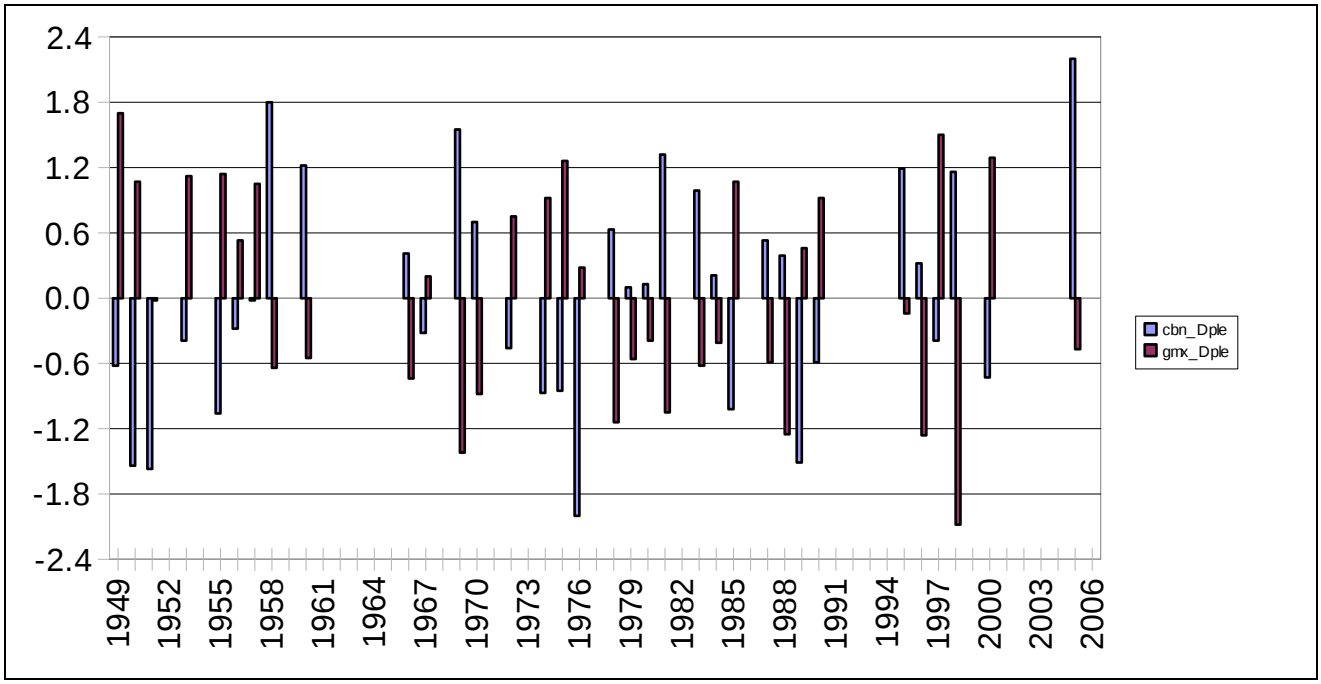


Figure 1. Time series of standardized SSTAs (°C) averaged over the Caribbean (blue) and the Gulf of Mexico (red) for IAS dipole years. The Caribbean area average is (66-88°W, 12-20°N) and the Gulf of Mexico area average is (76-96°W, 22-32°N) excluding the Pacific data.

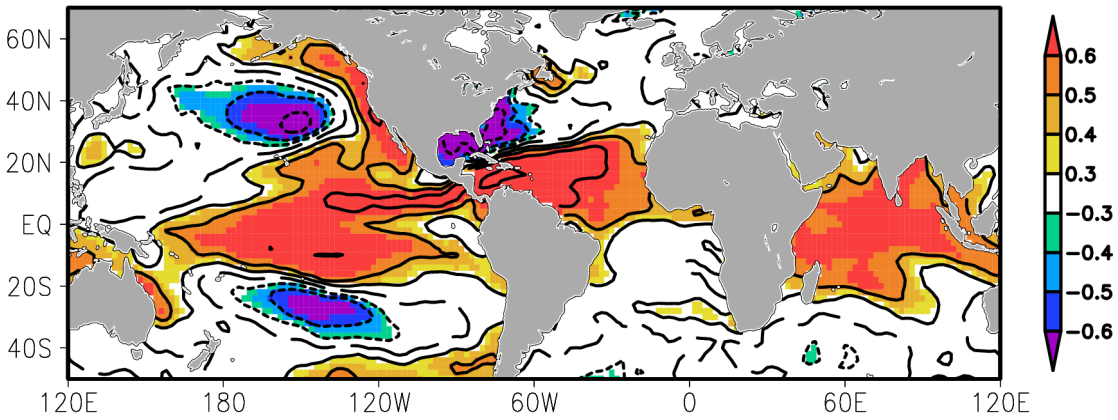


Figure 2. February-to-April correlation between the IAS SSTA dipole index and SSTAs (°C) from 1949 through 2006. The contour interval is 0.2 starting at ±0.3. The long-dashed contour is the zero correlation contour.

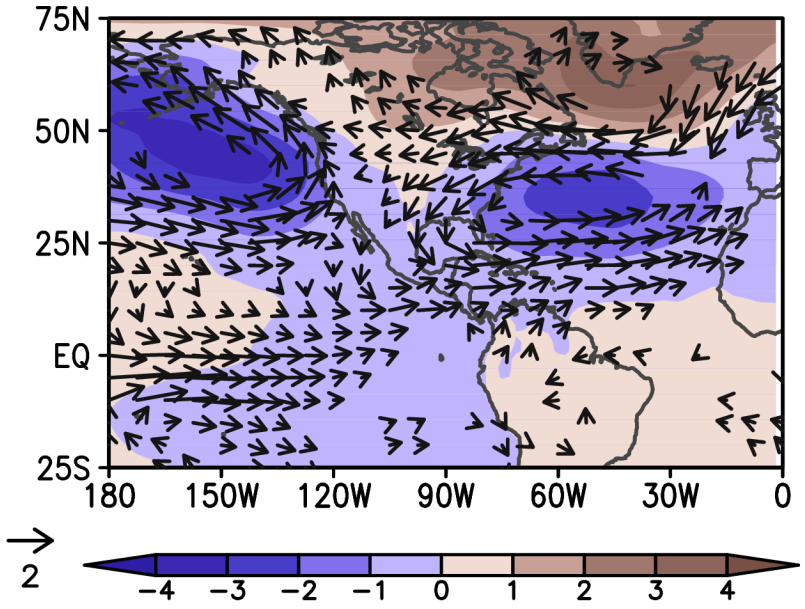


Figure 3. February-March regression of IAS SSTA dipole index onto 850-hPa wind (m/s; vectors) and surface pressure (hPa; shades) from 1949 to 2006.

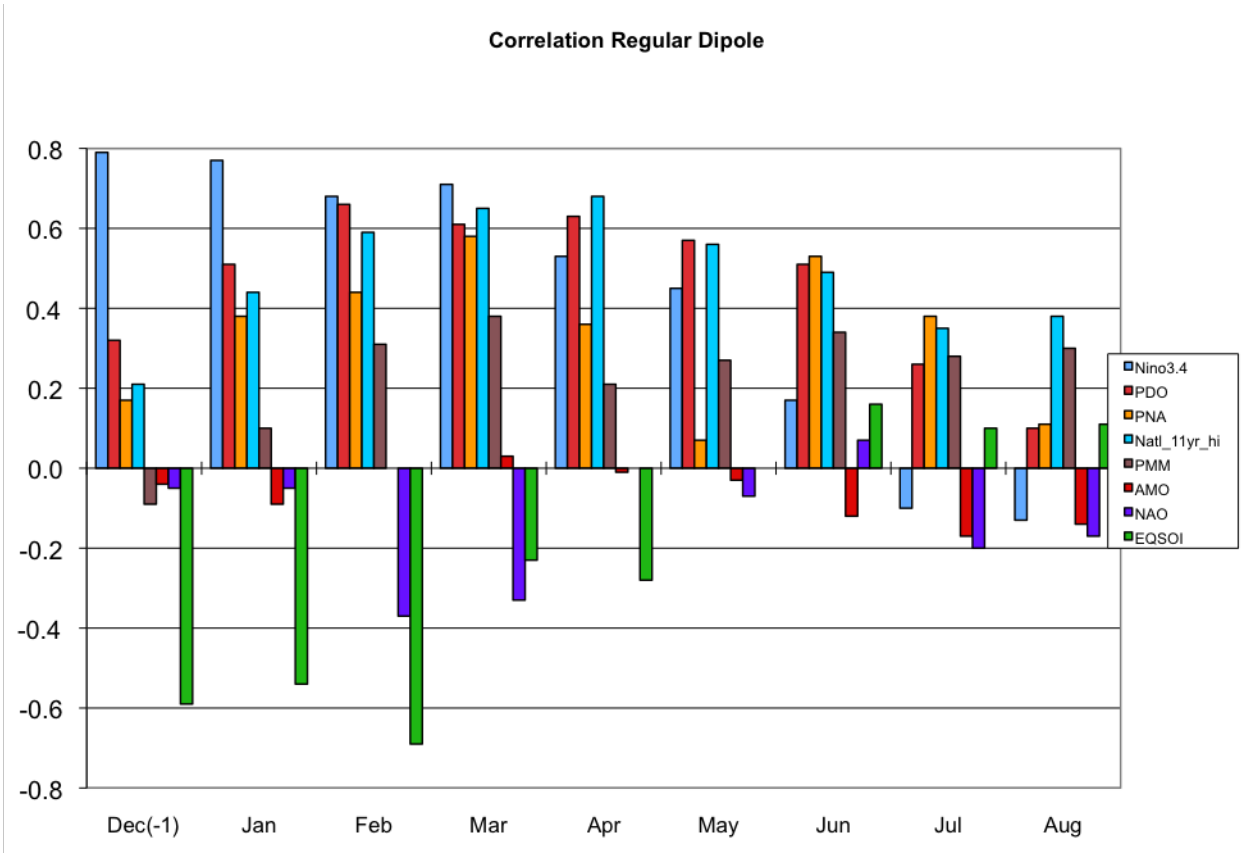


Figure 4. Correlation between the IAS SSTA dipole index and teleconnection indices in the Pacific (PDO, PNA, Nino3.4, EQSOI, PMM) and in the Atlantic (AMO, NAO, Natl 11-year high-pass).

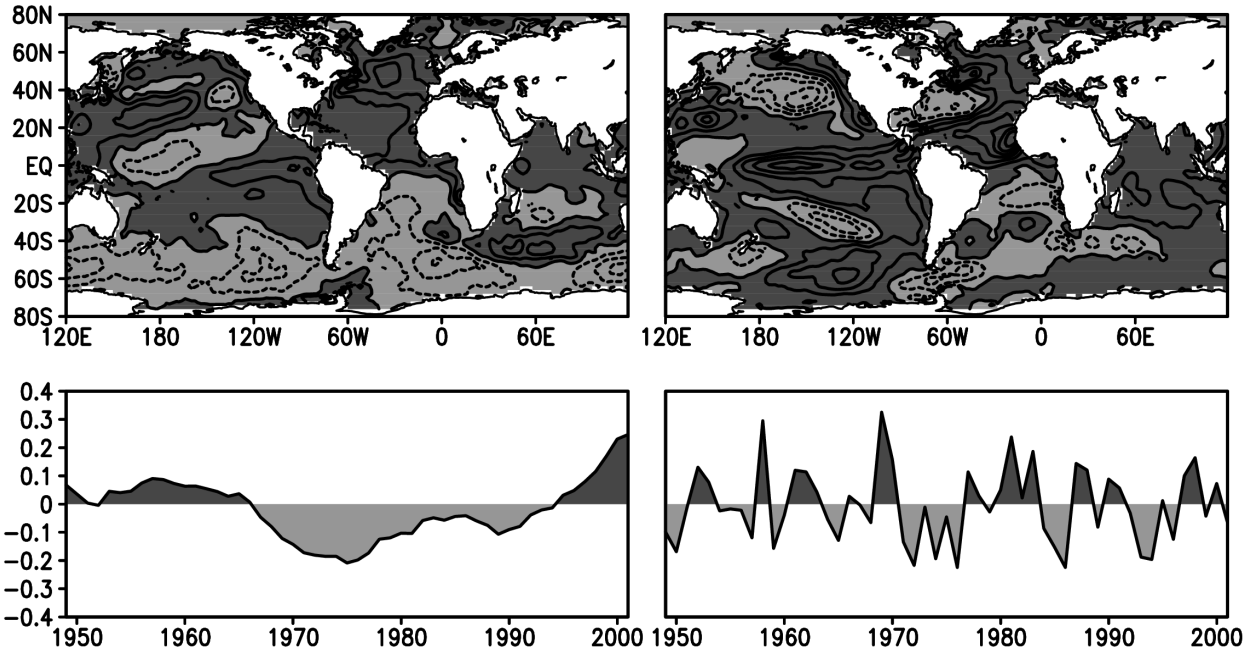


Figure 5. (Top) Regression of SSTA (°C) onto 11-year low-pass (left) and high-pass (right) North Atlantic SSTA index from 1949 to 2001. Contour interval is 0.1°C. Positive values are in dark gray and solid contours. Negative values are in light gray and dashed contours. (Bottom) Time series of the 11-year low-pass (left) and high-pass (right) index. (See text for explanation of indices).

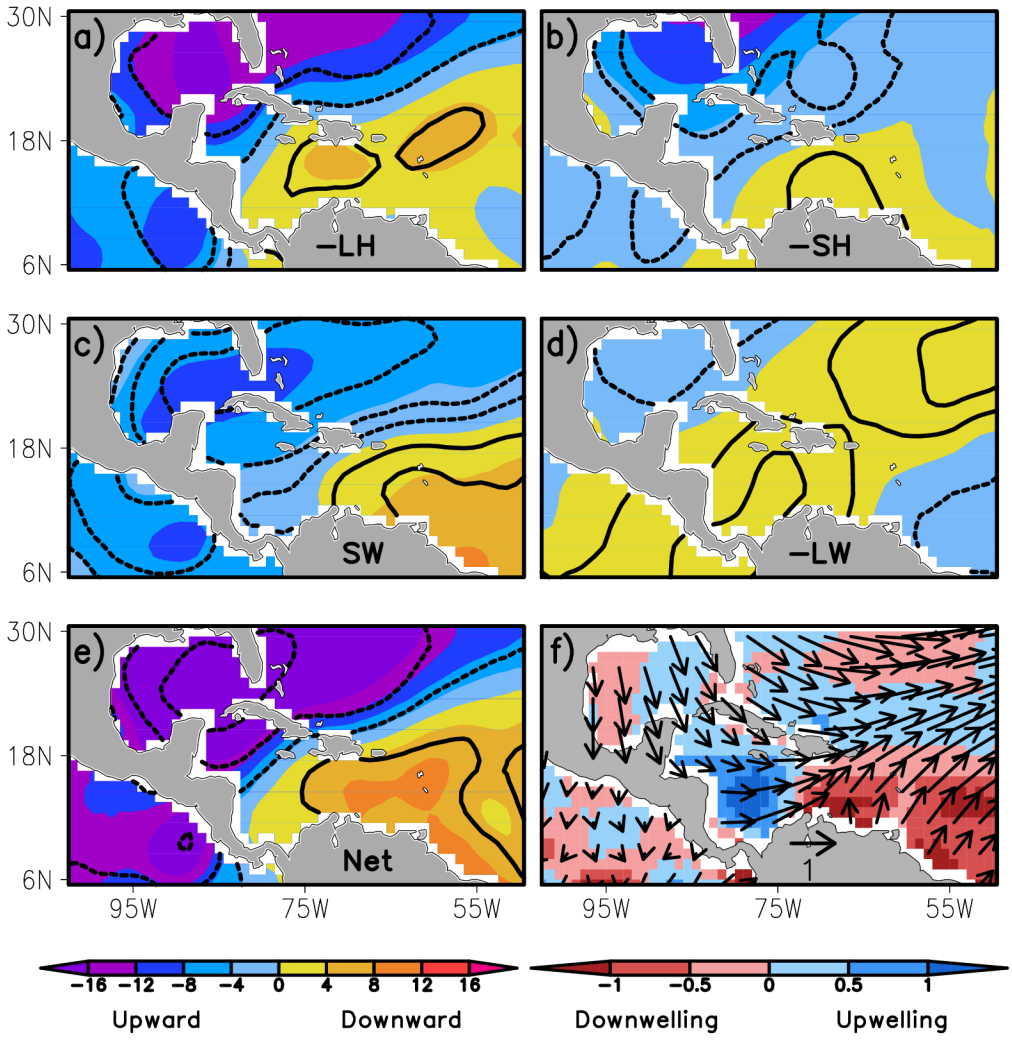


Figure 6. (a-e) January-to-March average regression (1949-2002) of turbulent and radiative air-sea heat fluxes ($W/m^2$) on dipole index (shades). Panels correspond to a) latent heat flux, b) sensible heat flux, c) shortwave, d) longwave, and e) net heat flux. The contours in panels a-e indicate the correlation at intervals of 0.2 starting at ±0.2 (negative correlations are shaded and positive correlations are solid). The contours in panel e indicate the ±0.3°C SSTA regression values. Panel f shows the regression of wind stress (arrows; $10^{-2}$ $N/m^2$) and Ekman pumping (shades; meters/month). The reference arrow is $1x10^{-2}$ $N/m^2$.

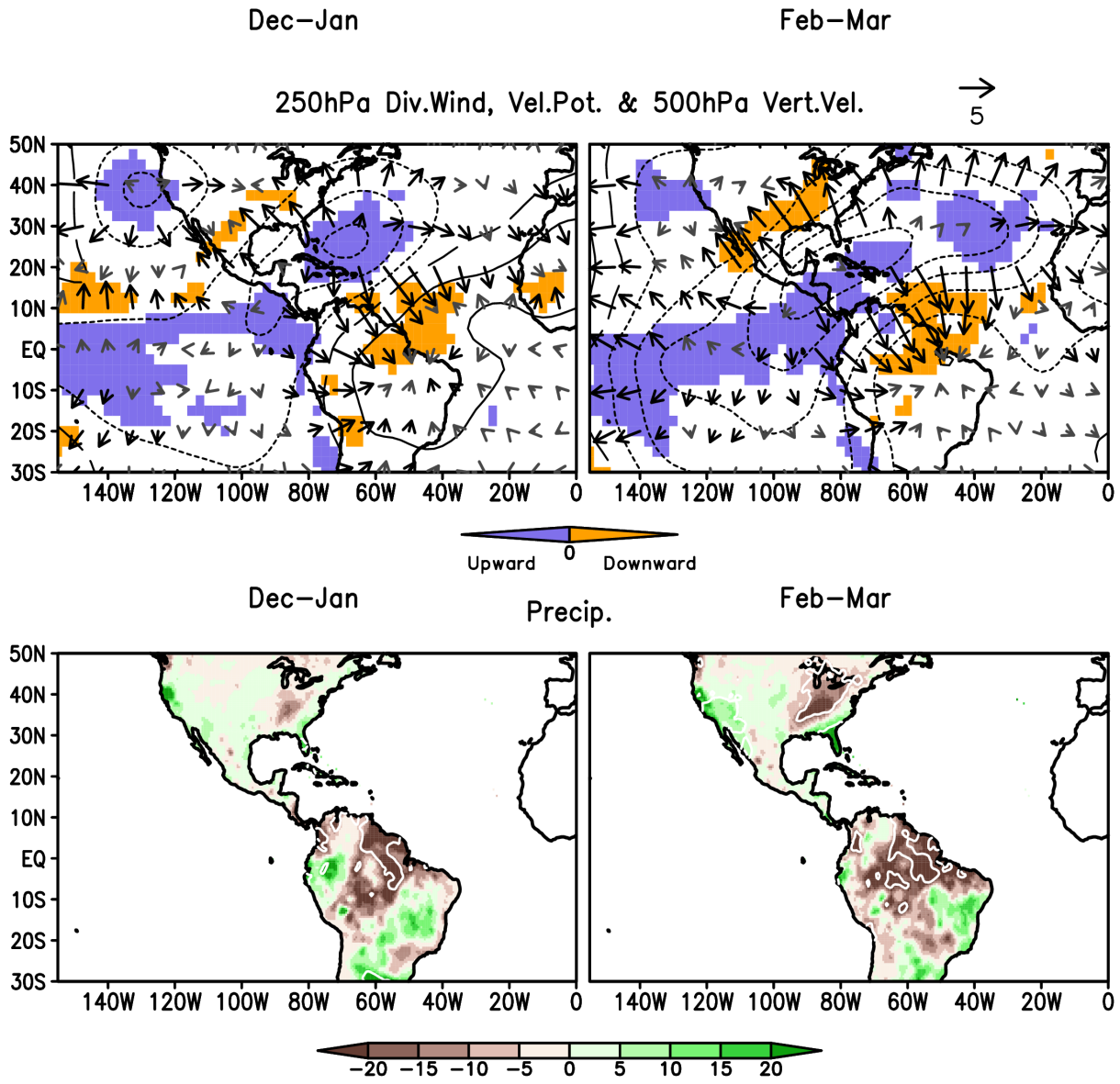


Figure 7. (Top) Regression of IAS SSTA dipole index onto upper-level (250-hPa) divergent wind (vectors) and velocity potential anomalies (contours). The reference arrow is $10^{-1}$ m/s. Black vectors are significant at the 95% level. The shades correspond to where the correlations between the dipole index and the 500-hPa vertical pressure velocity anomalies are greater than 0.3 or less than -0.3. The contour interval for velocity potential is $3x10^5$ $m^2/s$. (Bottom) Regression of precipitation anomalies (mm/month) with the IAS dipole index. The white contours encompass the regions where the regression is statistically significant at the 95% level.

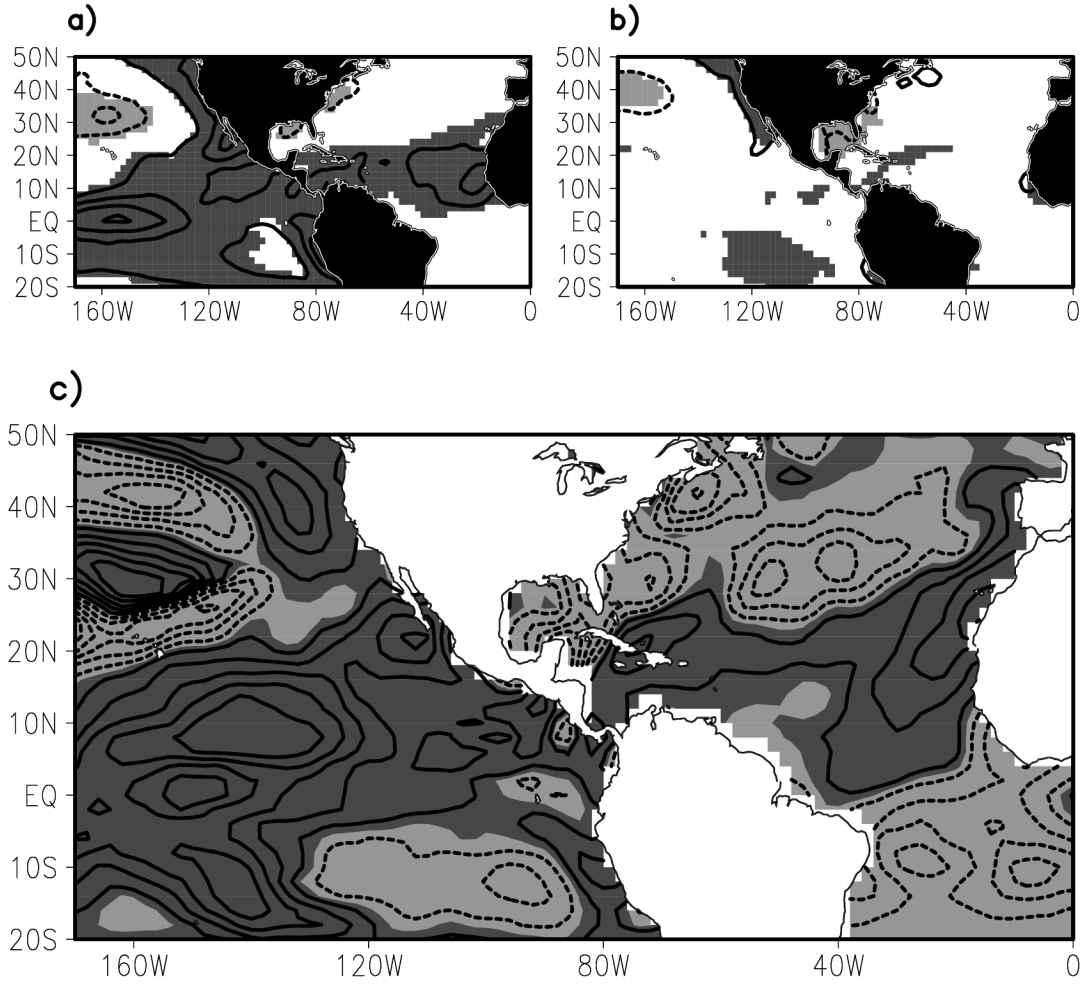


Figure 8. (a) March-April SSTA (°C) average regression of March Nino3.4 index when the March PNA extreme years have been excluded. (b) March-April SSTA (°C) average regression of March PNA index when the March Nino3.4 extreme years have been excluded. Contour interval is 0.2 starting at ±0.2. Values significant at the 95% level are shaded. (c) Difference in explained variance (%) of the March-April partial correlation between the PDO and SSTAs when the PNA index is controlled versus when the Nino3.4 index is controlled (see text for explanation). Contour interval is 2%. The zero contour has been omitted. Dark gray denotes positive values and light gray denotes negative values.

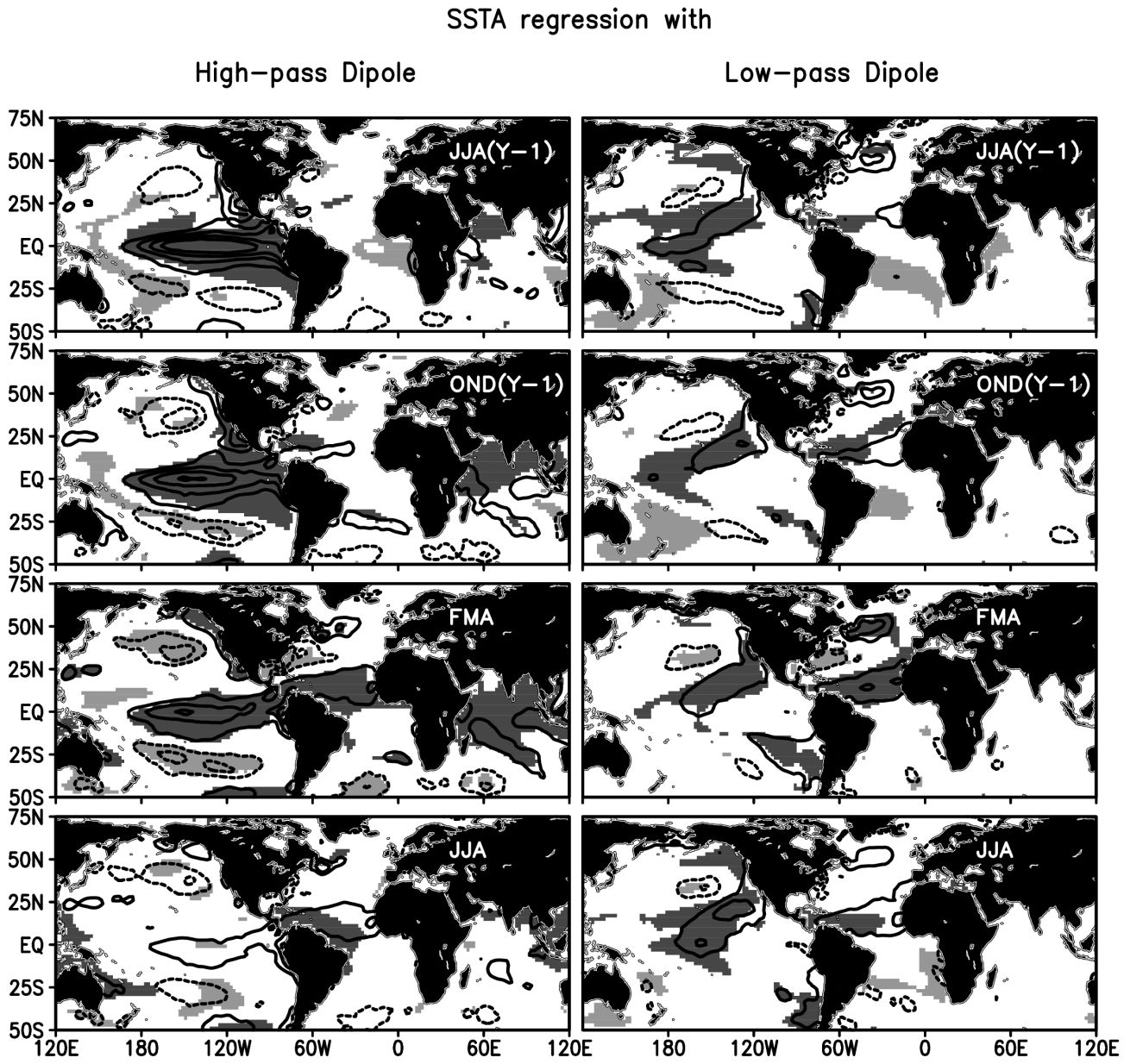


Figure 9. SSTA (°C) regression onto (left) 5-year high-pass dipole index and (right) 5-year low-pass dipole index for (from top to bottom) June-August of previous year, October-December of previous year, February-April and June-August. Contour interval is 0.2 starting at ±0.2. Values significant at the 95% level are shaded.

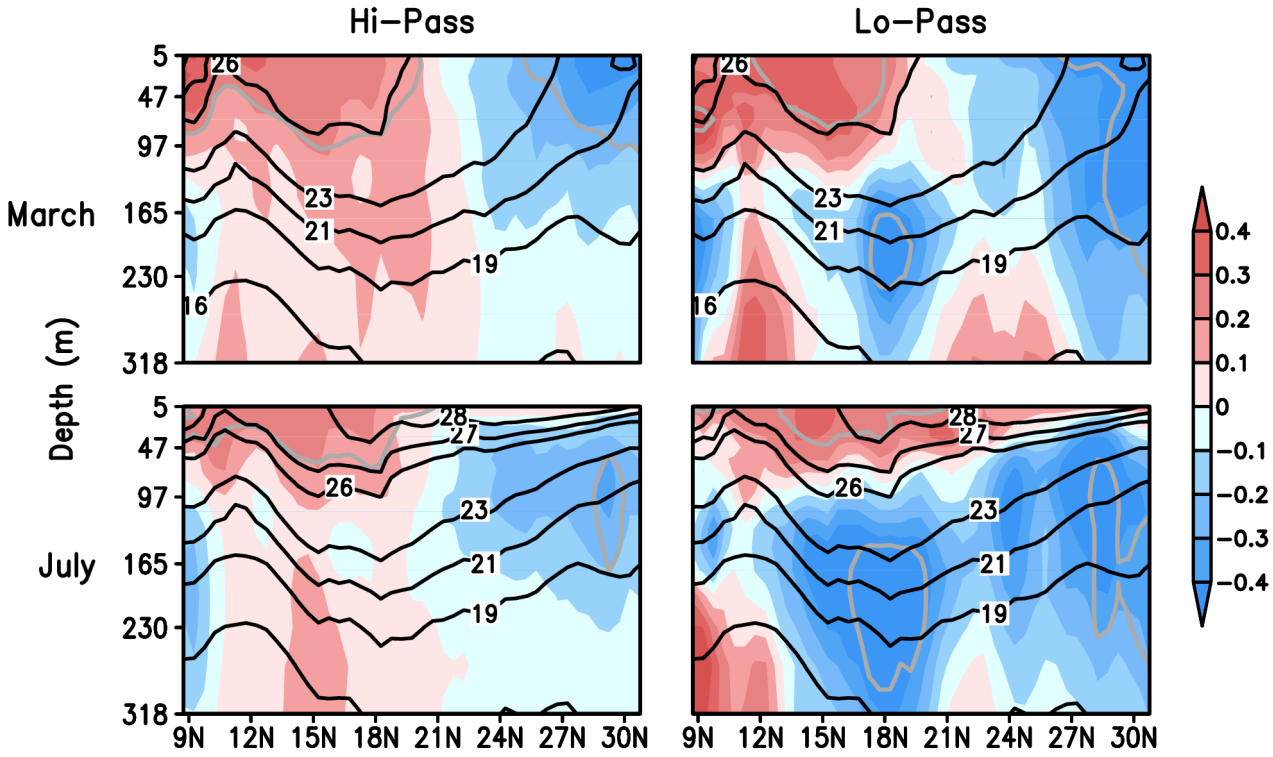


Figure 10. IAS zonal average of March (top) and July (bottom) regression of subsurface temperature (°C) for the 5-year high-pass (left) and low-pass (right) IAS spring dipole index. The zonal average is from the western boundary to 60°W. The black contours are the climatological isotherms (°C). The gray contours encompass the depths of significant regressions at the 95% level.

Table 1. Seasonal correlation between SSTAs in the Gulf of Mexico and in the Caribbean Sea. The Caribbean area average is (66-88°W, 12-20°N) and the Gulf of Mexico area average is (76-96°W, 22-32°N) excluding the Pacific data.

| Season | Correlation coefficient |
|---|---|
| November-January | -0.16 |
| February-April | -0.44 |
| May-July | 0.31 |
| August-October | 0.54 |

Table 2. Contingency table for instances when the SSTAs in the Gulf of Mexico (GMX) and in the Caribbean Sea (CBN) fall in their extreme tercile ranges or intertercile range. The chi-square is 19.43 with 4 degrees of freedom.

| | *GMX<-Tt* | *\|GMX\|<Tt* | *GMX>Tt* | *Total* |
|---|---|---|---|---|
| CBN>Tt | 10 | 4 | 8 | 22 |
| \|CBN\|<Tt | 7 | 11 | 2 | 20 |
| CBN<-Tt | 0 | 5 | 11 | 16 |
| **Total** | 17 | 20 | 21 | 58 |

Table 3. January-to-March average regression (1949-2002) of components of the turbulent air-sea heat fluxes ($W/m^2$) onto the dipole index. GMX is the Gulf of Mexico area average and CBN is the Caribbean Sea area average.

| Component | GMX | CBN |
|---|---|---|
| Wδq | -13.3 | 2.0 |
| Wδq' | -9.0 | 3.7 |
| W'δq | -4.3 | -1.7 |
| | | |
| WδT | -6.6 | 0.2 |
| WδT' | -10.9 | -0.3 |
| W'δT | 3.8 | 0.5 |

* As these are area averages the components may not balance each other.